




Article

Experimental Analysis of an Innovative Electrical Battery Thermal Management System

Luca Cattani ^{1,*}, Matteo Malavasi ¹, Fabio Bozzoli ¹, Valerio D'Alessandro ² and Luca Giammichele ²

¹ Department of Architecture and Engineering, University of Parma, Parco Area delle Scienze 181/A, 43124 Parma, Italy; matteo.malavasi@unipr.it (M.M.); fabio.bozzoli@unipr.it (F.B.)

² Department of Industrial Engineering and Mathematical Science, Università Politecnica delle Marche, 60131 Ancona, Italy; v.dalessandro@staff.univpm.it (V.D.); l.giammichele@staff.univpm.it (L.G.)

* Correspondence: luca.cattani1@unipr.it

Abstract: The aim of the present work is to develop and test an innovative cooling system for the thermal management of batteries for electric vehicles (EVs). At present, the technology most used for electric propulsion is based on lithium-ion cells. The power supply unit must often deliver a large amount of power in a short time, forcing the batteries to produce a considerable amount of heat. This leads to a high working temperature that can cause a sharp decrease in the battery performance or even a malfunction. Moreover, their working outside of the prescribed temperature range (20–40 °C) or with a significant temperature gradient across the battery meaningfully accelerates their aging or breakage. In this case, a battery thermal management system (BTMS) is necessary to allow the batteries to work as efficiently as possible. In the present work, a pulsating heat pipe with a three-dimensional structure is proposed as cooling technology for a battery pack. At first the performance of the proposed PHP is evaluated in a dedicated experimental setup under different boundary conditions and a wide spectrum of power input values. Then the PHP is tested by applying, as load at the evaporator section, heat power distribution corresponding to three different discharging processes of a battery. These tests, directly referring to an applicative case, show that the proposed 3D PHP has an optimal cooling ability and the possibility to offer a powerful solution for electrical battery thermal management.

Keywords: pulsating heat pipes; batteries for electric vehicles; thermal management system



Citation: Cattani, L.; Malavasi, M.; Bozzoli, F.; D'Alessandro, V.; Giammichele, L. Experimental Analysis of an Innovative Electrical Battery Thermal Management System. *Energies* **2023**, *16*, 5071. <https://doi.org/10.3390/en16135071>

Academic Editors: Iztok Golobič and Matic Može

Received: 23 May 2023
Revised: 21 June 2023
Accepted: 24 June 2023
Published: 30 June 2023



Copyright: © 2023 by the authors. Licensee MDPI, Basel, Switzerland. This article is an open access article distributed under the terms and conditions of the Creative Commons Attribution (CC BY) license (<https://creativecommons.org/licenses/by/4.0/>).

1. Introduction

One of the main challenges of the 21st century is represented by the transition to sustainable mobility. A prominent role in this scenario is played by the development of electric propulsion in vehicles. It constitutes a crucial topic in the world, taking on a major role in the economic, social and climate strategies. Electric vehicles (EVs) allow significant reduction in the environmental impact by decreasing emissions of pollutants into the atmosphere to zero. Furthermore, they also lead to a reduction in the acoustic impact of vehicles in high population density zones or near these areas. At present, the technology most used for electric propulsion is based on lithium-ion (Li-ion) cells [1–3]. Although the industrial market is already under development, it is in an experimental phase and electric traction systems still require accurate improvement and development. From the electrochemical perspective Li-ion cells have reached a satisfactory level of optimization, however, one of the bigger and still open challenges is represented by the thermal management of the batteries. Indeed, the power supply unit must often deliver a large amount of power in a short time, forcing the batteries to produce a considerable amount of heat. This leads to a high working temperature that can cause a sharp decrease in the battery performance or even a malfunction. Moreover, when the batteries work outside of the prescribed temperature range (20–40 °C) or with a significant temperature gradient,

it meaningfully accelerates their aging [4,5]. In this case, a battery thermal management system (BTMS) is necessary to allow the batteries to work as efficiently as possible and means extending their useful life. Therefore, the environmental impact of Li-ion cell production and disposal is reduced if compared with the operative period. In the open literature and in the industrial applications, various cooling strategies are adopted. The easiest one comprises air-cooling systems often aided by heat sinks/fins [6–8]. These kinds of BTMS, however, are not suitable for high-power vehicles. Liquid chilling approaches are more efficient for EVs because of their higher thermal capacity. This methodology adopts a single- or two-phase refrigerant [9–12], that streams inside a heat exchanger, enveloping the power module. In this arrangement, despite its efficacy, an additional thermal resistance is added due to the heat exchanger's presence. For these reasons, a directly cooling BTMS could be an interesting solution for EVs' Li-ion battery cells [13,14]. Moreover, in recent studies the performance of innovative BTMSs such as phase change materials [15,16] and heat pipes was investigated [17,18]. The ideal BTMS should be able to operate safely and robustly [19] within the restricted space available in EVs, provide the necessary cooling in terms of maximum temperature and uniformity of distribution, and be low cost. Among the previously cited cooling techniques the liquid-based approaches in a two-phase state are the most effective but normally they require an outside power source and their energetic and economical price is not trivial. One fascinating solution that brings together a passive operating behavior and a small economical expense is offered by the implementation of pulsating heat pipes (PHPs). The PHPs fit into the class of passive two-phase capillary-driven circuits. PHPs are extremely easy and cost effective compared to other heat transport devices [20]. They cope with elevated heat power due to the phase change phenomena and to the substantial sensible heat transfer carried out by the continual pulsations [21,22]. Moreover, PHPs are totally passive, so they avoid electric energy consumption and allow a compact power supply unit, and their adoption in the battery pack could also represent a promising approach to attain a uniform temperature. In addition, effective heat dissipation is a critical concern, not just limited to Li-ion batteries. It holds even greater significance for emerging technologies such as batteries employing solid-state electrolytes, where higher energy density is expected [23,24]. In fact, these batteries experience potentially hazardous temperature rises under conditions of elevated ambient temperature or high discharge currents [25]. In the present work a 3D PHP is realized to envelope a practical application represented by a nine-cell battery pack with a nominal voltage of 9.6 V and a capacity of 5.4 Ah [26]. At first the performance of the proposed PHP is evaluated in a dedicated experimental setup under different boundary conditions and a wide spectrum of power input values. Then the PHP is tested by applying, as load at the evaporator section, the power distribution corresponding to the heat generated for three different discharging processes by the battery tested in [26]. The three discharging curves referred to different fully discharging processes with a constant operating current at various values of C-rates (i.e., C1, C2 and C3).

2. Experimental Setup

The PHP studied here comprised three sections: the evaporator, the condenser and the adiabatic section characterized by a length of 9 cm, 7 cm and 3 cm, respectively, as shown in Figure 1. Moreover, as seen from Figure 1 the studied PHP presented a 3D structure characterized by turns on 3 sides to adequately embrace the battery without hindering the assembly. The device was fabricated by bending a stainless-steel pipe with internal and external diameters of 1.76 mm and 3.18 mm, in 11 turns. The tube was bent by using a Swagelok[®] hand tube bender to avoid flattening the tube, which represents a classical problem when bending a pipe with a small diameter. Stainless-steel pipes were employed since they are easy to purchase and cheap, two core factors for real industrial applications. The pipe was vacuumed and afterward not completely charged (filling ratio = 50%) with HFC-134a. The filling ratios between 20% and 80% let the device work as a true PHP [24]. The filling ratio (FR) represents the fraction by volume of the PHP which is initially filled

with the liquid (evaluated at room temperature). The fluid volume was estimated from the liquid density at environmental temperature and from the fluid mass, which was determined by weighing the PHP with and without the fluid using a high-precision balance (KERN EG 620 3NM). Furthermore, the empty device was experimentally investigated to analyze the difference from the totally conductive mode. The charging process was performed through the setup reported in Figure 2.

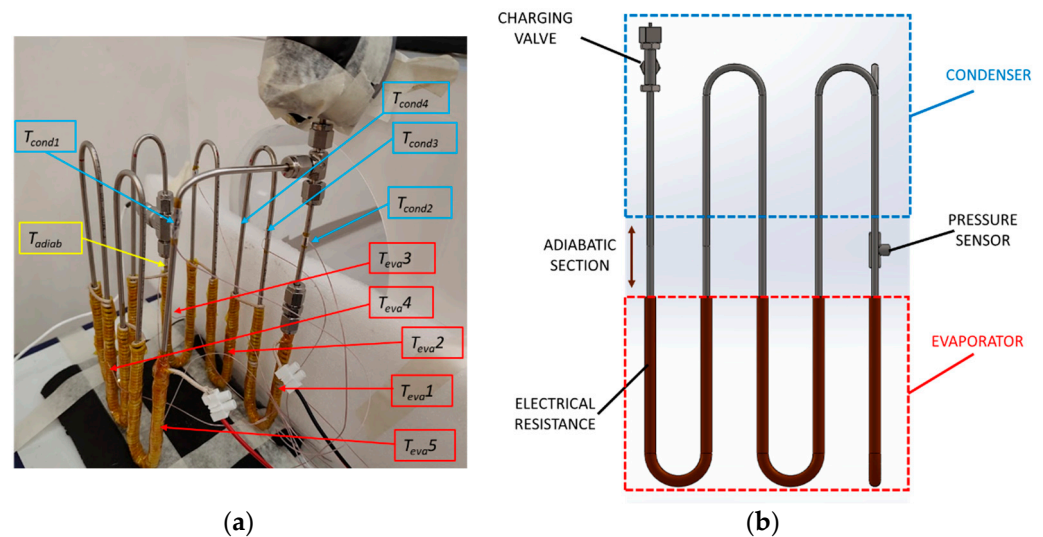


Figure 1. Photo (a) and 2D sketch (b) of the PHP.

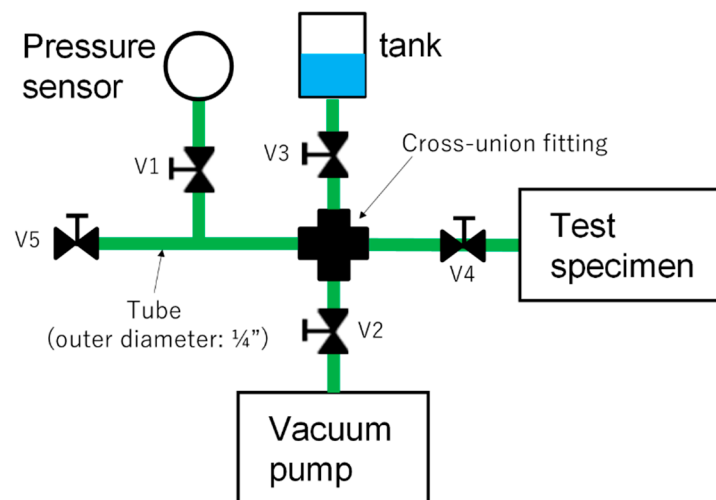


Figure 2. Vacuum and filling system.

During the emptying of the PHP using a vacuum pump (Agilent DS40M.), valves V3, V4 and V5 (Figure 2) were closed. The obtainment of a sufficient degree of void was checked through a vacuum gauge controller (RGC-150 Agilent). In the next phase valves V1, V2 and V5 were closed, and the device was charged with the working fluid.

The heat power at the evaporator section was furnished by Joule effect by means of a wire resistor wound around the tubes along the whole evaporator length and connected to a power supply. The condenser zone was cooled by means of air under different convection conditions, i.e., natural convection and forced convection at different air velocity values (1 and 2.5 m/s). For the tests in forced convection a wind tunnel was adopted as shown in Figure 3. The air velocity was measured with an anemometer (TESTO 435), it was measured corresponding to several points of the 3D structure of the PHP and a maximum difference lower than 15% was found between the different measures. The temperature of

the evaporator and the condenser was detected through five and four T-type thermocouples, respectively (see Figure 1a). All the thermocouples were fixed on the PHP's external wall by employing aluminum and Kapton[®] (DuPont, Washington, DC, USA) tapes. Additionally, the temperature at the adiabatic section and in the atmosphere was detected by T-type thermocouples. The fluid pressure at the adiabatic section was measured by a miniature pressure transducer (Kulite XTL-190S-500 PSI SG), directly inserted in the fluid stream and positioned in series with an in-line amplifier (Kulite[®] KEA-C-1B, Leonia, NJ, USA).

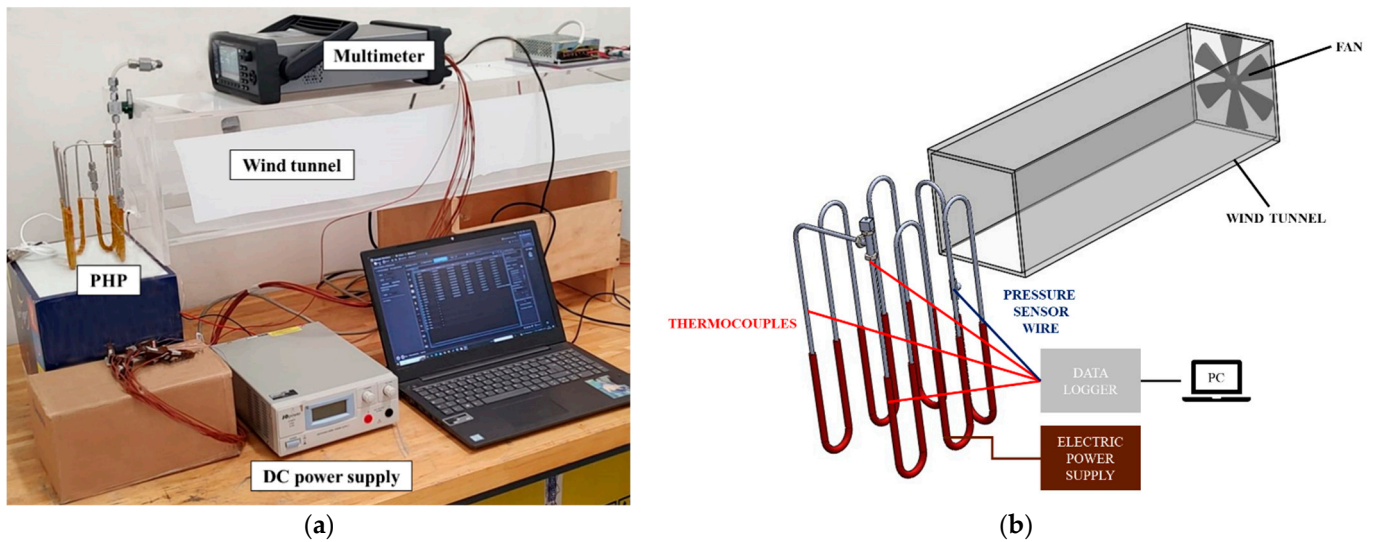


Figure 3. Photo (a) and sketch (b) of the experimental setup.

The 3D PHP was sized considering a practical application constituted by a 9-cell battery pack with a nominal voltage of 9.6 V and a capacity of 5.4 Ah [26]. The element considered here, for larger vehicles, is certainly insufficient but lends itself to modular scalability, making it suitable for many conditions. Clearly, the composition of multiple modules could generate additional issues regarding the system's thermal management space requirements, and this element will be studied in future work. In the present study the battery was simulated from the thermal point of view by the wire resistor described earlier. However, to better understand the forecasted coupling of the PHP with the battery a sketch is reported in Figure 4.

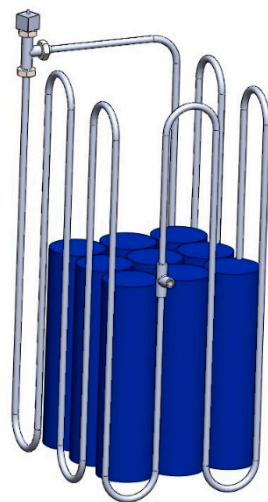


Figure 4. Sketch of the battery–PHP coupling.

At first the performance of the proposed PHP was evaluated under different boundary conditions and a wide spectrum of power input values. During these tests, a stepwise heating input was supplied to the evaporator from 1 W to 90 W by a DC power supply. The measurements were gathered by a data acquisition system (AGILENT 34970A), for every power load once the PHP accomplished the pseudo-steady state. Then the PHP was tested by applying, as load at the evaporator section, the power distribution corresponding to 3 different discharging processes of the battery tested in [26]. The 3 discharging curves referred to different fully discharging processes with a constant operating current at various values of C-rates (i.e., C1, C2 and C3). The measurement uncertainties of the T-type thermocouple and the voltage and the current of the power supply were ± 0.1 °C, $\pm 0.05\%$ (full-scale V) and $\pm 0.05\%$ (full-scale A), respectively.

3. Results and Discussion

3.1. Staircase Function Load

During these tests, a staircase function heating input was supplied to the evaporator from 1 W to 90 W. At first the thermal performance of the proposed device was evaluated in terms of average thermal resistance R_{eq} as reported by several authors in the literature [27–30]:

$$R_{eq} = \frac{\bar{T}_{eva} - \bar{T}_{cond}}{Q} \quad (1)$$

where \bar{T}_{eva} is the average of the temperatures measured by the thermocouples at the evaporator as it is for \bar{T}_{cond} regarding the condenser, and Q is the electric power input supplied to the wire heater. The evaporator and condenser temperatures were obtained by averaging the measured values, at constant load, over a 600 s period; these values were collected only when a pseudo-steady state was reached. The uncertainty in thermal resistance was estimated by means of the propagation of error method [31]; the maximum uncertainty on the thermal resistance was $\pm 10\%$.

The performance of the proposed PHP was tested considering air cooling at the condenser by evaluating three different flow conditions, i.e., natural convection, forced convection at 1 m/s and forced convection at 2.5 m/s. In Figure 5 the temperature distributions measured by all the thermocouples together with the pressure signal versus the time for the input load range of 1–78 W for the case of natural convection are reported.

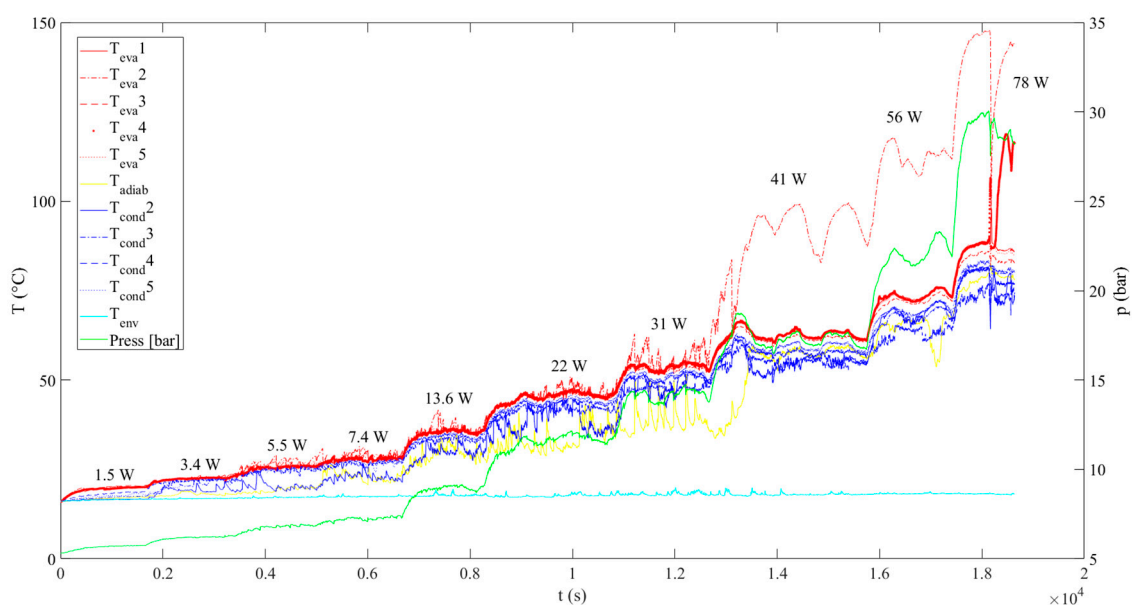


Figure 5. Temperature distributions vs. time for the case of natural convection at the condenser.

Figure 6 shows the overall thermal resistance versus the heating input for the case of natural convection at the condenser together with the results obtained with the empty device. When the device is empty it operates as a purely conductive device and its thermal resistance is practically invariant ($\sim 2^\circ\text{C}/\text{W}$) with the power load. When the PHP is charged with the working fluid, the transport phenomena (thermally induced pulsations) decrease the average thermal resistance more than five times compared to the empty PHP. From Figure 5 it is interesting to notice that the startup condition seems to appear very early; between 3 and 5 W the first significant oscillations rise in the temperature distribution. Shortly after imposing 3.4 W input power, it can be seen that the condenser temperatures approached those of the evaporator, indicating an increase in the heat transfer capacity of the device. This is also confirmed by the sudden decrease in the average thermal resistance for the same power input values observable in Figure 6. The vertical operation is certainly helping the arising of the startup condition. The fact that the liquid phase is pushed to the condenser more effectively if the device works in the bottom-heated mode (evaporator at the bottom) or gravity-assisted mode is confirmed in the literature [24,32]. When the pulsation onset and the fluid inertia have a significant role, the PHP demonstrates excellent thermal performances, with even a thermal resistance that is 10 times lower compared to the empty device case for the power input range of 10–30 W. After this range it is possible to see a slight increase in the thermal resistance; this is probably due to the fact that the quantity of vapor is approaching the dry-out condition in some of the turns and the heat dissipated at the condenser with the natural convection mechanism is not sufficient to allow the recondensation of the fluid in all the turns. This is also confirmed by the temperature distribution of the thermocouple T_{evn2} in Figure 5 that from the power input of 41 W reaches values significantly higher than the other sensors, highlighting that that branch is probably mostly filled by vapor even if the condition is not of a complete dry-out since it is possible to observe various drops in the temperature distribution due to flow reversal phenomena of liquid from the condenser.

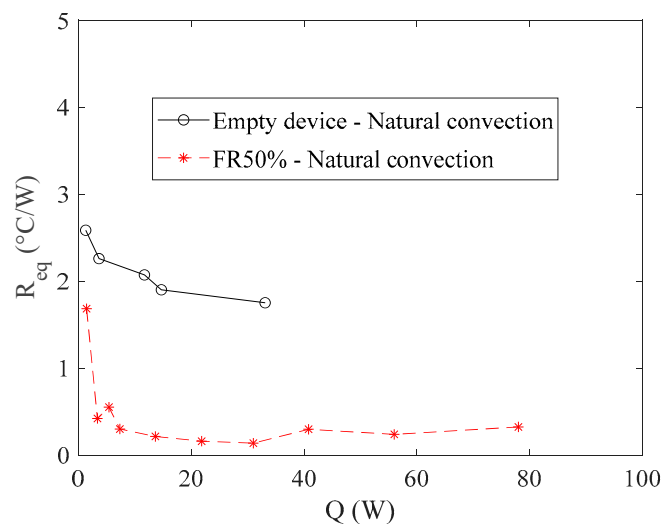


Figure 6. Thermal resistance for the case of natural convection at the condenser.

With the adoption of forced convection at the condenser this local phenomenon of non-uniformity of temperature at the evaporator disappears as is testified by Figure 7 where the temperature distribution measured by all the thermocouples versus the time for the input load range of 1–90 W for the case of forced convection with air velocity of 1 m/s is reported.

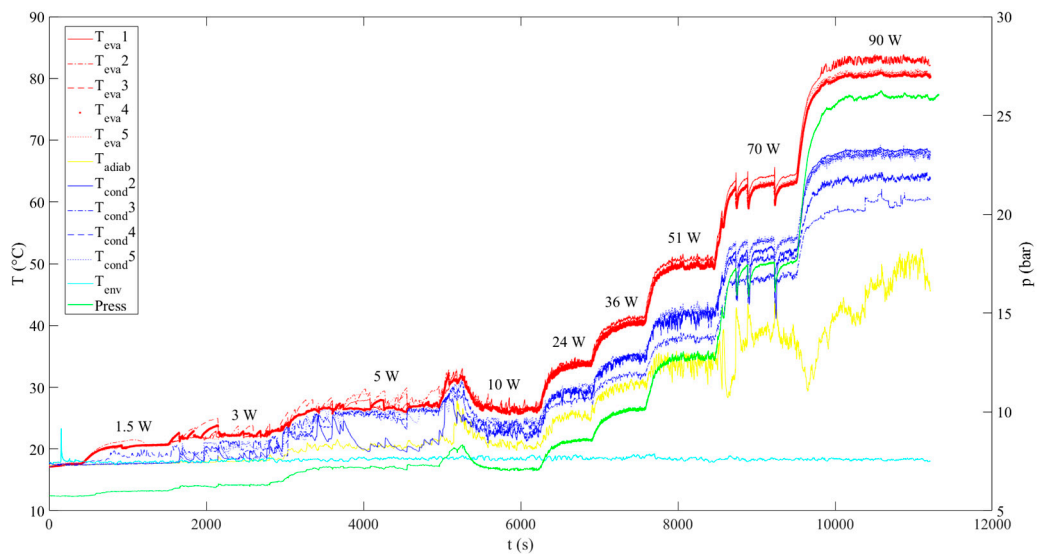


Figure 7. Temperature distributions vs. time for the case of forced convection ($v = 1 \text{ m/s}$) at the condenser.

In addition, in this case the activation of the device occurs in the range of power input values of 3–5 W. From the startup, clear oscillation phenomena could be observed from the sensor measurements for all the heat loads. The complete activation of the device is also testified by the lower temperatures reached at the evaporator with respect to the case of air natural convection at the condenser. What was observed for the case of forced convection with air velocity of 1 m/s was also detected for the case of air velocity of 2.5 m/s where the heat transfer condition at the condenser is even more favorable.

Then, in Figures 8 and 9, the comparisons between the overall thermal resistance and the average evaporator temperature for all the configurations considered, respectively, are represented. For every analyzed case the experimental tests have been repeated at least 3 times to verify the repeatability of the phenomenon and the robustness of the data, and all the experiments have been conducted at environmental temperature equal to 18 °C. To obtain this ambient condition the experimental tests were performed inside a climatic chamber of 4.0 m × 2.3 m × 2.6 m with 60 mm thick panels that, thanks to an air handling unit (CTA series CETRA air flowrate 500 m³/h), allowed simulation of ambient conditions in the interval of 10–30 °C.

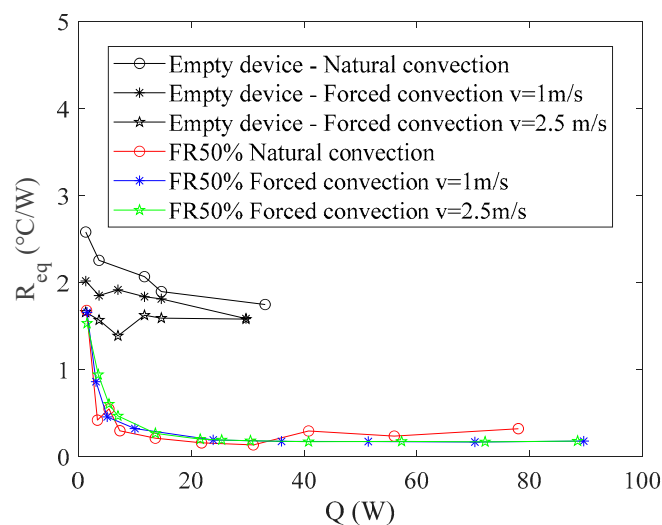


Figure 8. Thermal resistance.

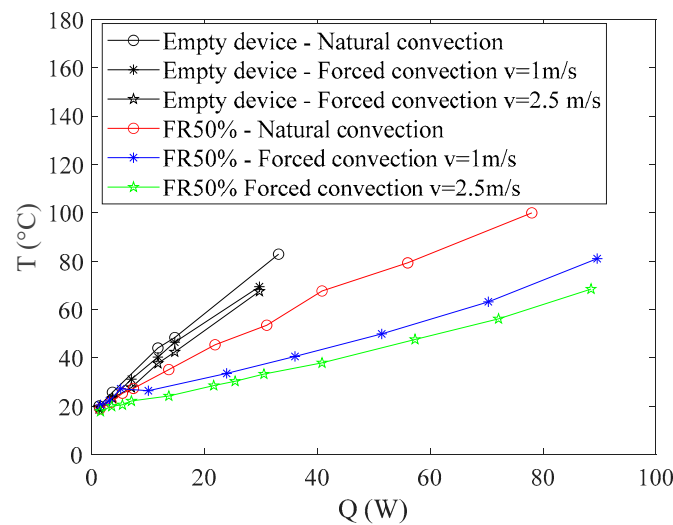


Figure 9. Average evaporator temperature.

It is possible to see from Figure 7 that the two configurations with forced convection at the condenser, as predicted, perform better in terms of overall thermal resistance of the device. Additionally, the natural convection configuration shows promising performance with a thermal resistance that is only slightly higher than the ones found for forced convection cases in the range of 40–80 W, but it is characterized by significantly higher temperature values at the evaporator (Figure 9) and by a non-negligible non-uniformity between the different turns as shown in Figure 5. This aspect could be crucial for the application under study since, as already explained in the Introduction section, working outside of the prescribed temperature range (20–40 °C) or with a significant temperature gradient across the battery meaningfully accelerates its aging or could even cause premature breakage.

3.2. Discharging Process at Mild Environmental Temperature

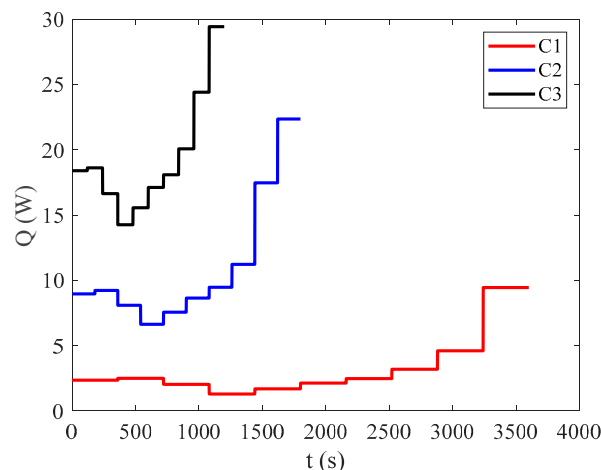
To investigate the efficiency of the proposed cooling system in real-world battery operating conditions, the device was tested by applying, as power load at the evaporator section, the power distribution corresponding to the heat generated for three different discharging processes by the battery pack presented in [26]. The three discharging curves referred to different fully discharging processes with a constant operating current at various values of C-rates (i.e., C1, C2 and C3). The values of the current at the three different C-rates are reported in Table 1 and the heat power generated by the battery during the discharging process, as determined in [33], is shown in Figure 10. The Bernardi equation [34] was used to evaluate the heat generation of a single cell:

$$Q = I \cdot (V - U_{OC}) + I \cdot T \cdot \frac{\partial U_{OC}}{\partial T} \quad (2)$$

where I is the discharge current, V is the cell potential, T is the battery surface temperature (expressed in K), U_{OC} is the open circuit potential and $\partial U_{OC}/\partial T$ is the entropic heat coefficient (EHC). Both EHC and U_{OC} were measured for the battery under testing with specific tests described in [33] for every 10% of state of charge. The other terms of Equation (1) (i.e., current, cell potential and surface temperature) were measured during full discharge tests at the three C-rates reported in Table 1 for a single cell. The heat power presented in Figure 10 is the result of Equation (2) multiplied by the number of cells used in the battery pack under investigation.

Table 1. Constant current discharge process [23].

C-Rate	Current [A]	Time [s]
1	5.4	3600
2	10.8	1800
3	16.2	1200

**Figure 10.** Discharging curves.

The discharging curves have been adopted as conditions to evaluate the applicability of the proposed thermal management system since Li-ion cells are usually subjected to very stressful operating conditions during the battery discharge phase.

The three discharging curves were applied at the evaporator for all the considered boundary conditions at the condenser. In Figure 10 the average temperature at the evaporator and at the condenser for C1, C2 and C3 discharge curves for the case of natural convection is reported. The tests were performed at an ambient temperature of 18 °C. To avoid malfunctioning or possible runaway the goal for the BTMS is trying to keep the maximum temperature under 40 °C. This achievement is reached for the two curves at C1 and C2 while, at C3, where a higher power must be dissipated, the evaporator temperature surpasses 45 °C.

In the case of C1 the power to be dissipated is very low and the device can keep the temperature under the upper limit even if it is not working in oscillating mode for the first 3000 s. Indeed, from Figure 11a it is possible to define the PHP activation of the device only around $t = 3000$ s where both the temperature at the evaporator and at the condenser exhibits appreciable oscillations. It is worth noting that in the first 3000 s the device is neither working in oscillating mode nor in pure conductive mode as happened with the empty device. In the case of pure conductive mode, the evaporator curve will be characterized by a significant increasing trend while from Figure 11a it is possible to see a plateau distribution of temperature in the interval of 500–3000 s.

At this stage the device is probably working as a thermosyphon where the motion engine is represented exclusively by the buoyancy and gravity forces. The heat transfer due to the latent heat of evaporation and condensation is still present but it is missing, with respect to the PHP case, the significant sensible heat transferred thanks to the high-frequency oscillations that characterize the PHP's pulsating working mode. The distribution of the temperature at the evaporator and the condenser is indeed characterized by a smoother trend [35]. For the C2–C3 rates the activation occurs before, i.e., around 200 s, but it is not enough to keep the temperature under the upper limit for the C3 case. The bottleneck in this case is due to the low heat transfer coefficient between the tubes at the condenser and in the environment since natural convection is usually characterized by convective heat transfer coefficient in the range of 10–25 W/m²°C. To overcome this issue,

it is necessary to increase the heat transfer surface. This problem is not present in the case of forced convection at the condenser. In Figures 12 and 13 the average temperatures at the evaporator and at the condenser for C1, C2 and C3 discharge curves for the case of forced convection are reported for air velocity $v = 1 \text{ m/s}$ and $v = 2.5 \text{ m/s}$, respectively. These values are quite conservative with respect to the ones achievable during the moving of an electric vehicle, i.e., cars, planes or even bicycles.

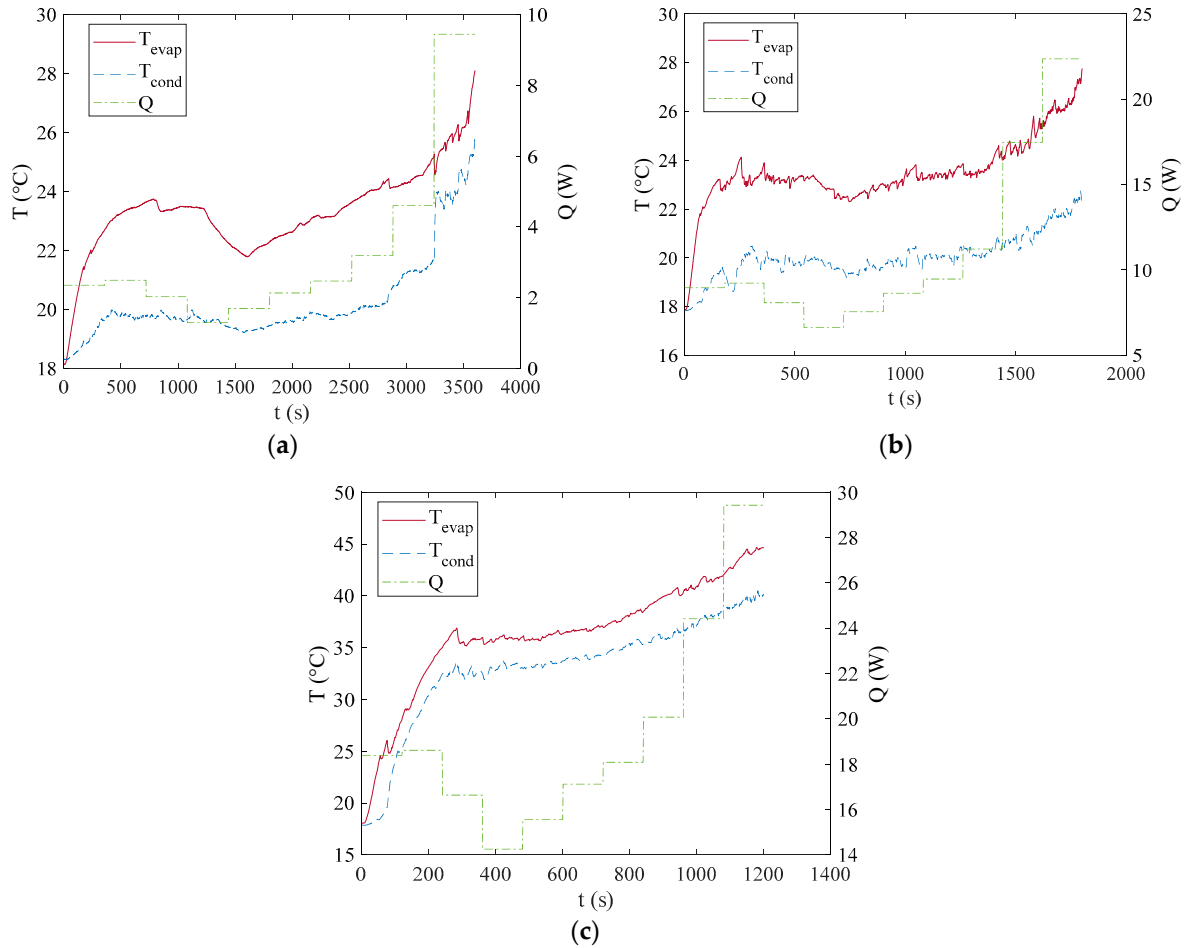


Figure 11. Average temperature at the evaporator and at the condenser for C1 (a), C2 (b) and C3 (c) discharging curves for the case of natural convection.

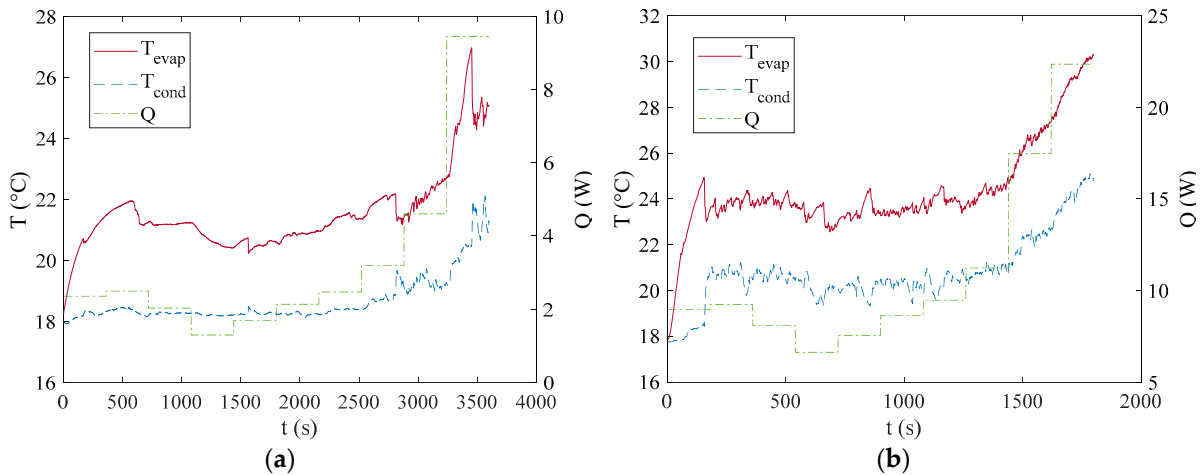


Figure 12. Cont.

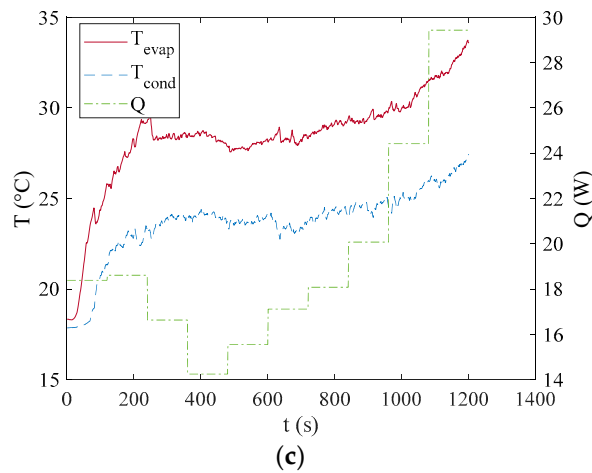


Figure 12. Average temperature at the evaporator and at the condenser for C1 (a), C2 (b) and C3 (c) discharging curves for the case of forced convection ($v = 1$ m/s).

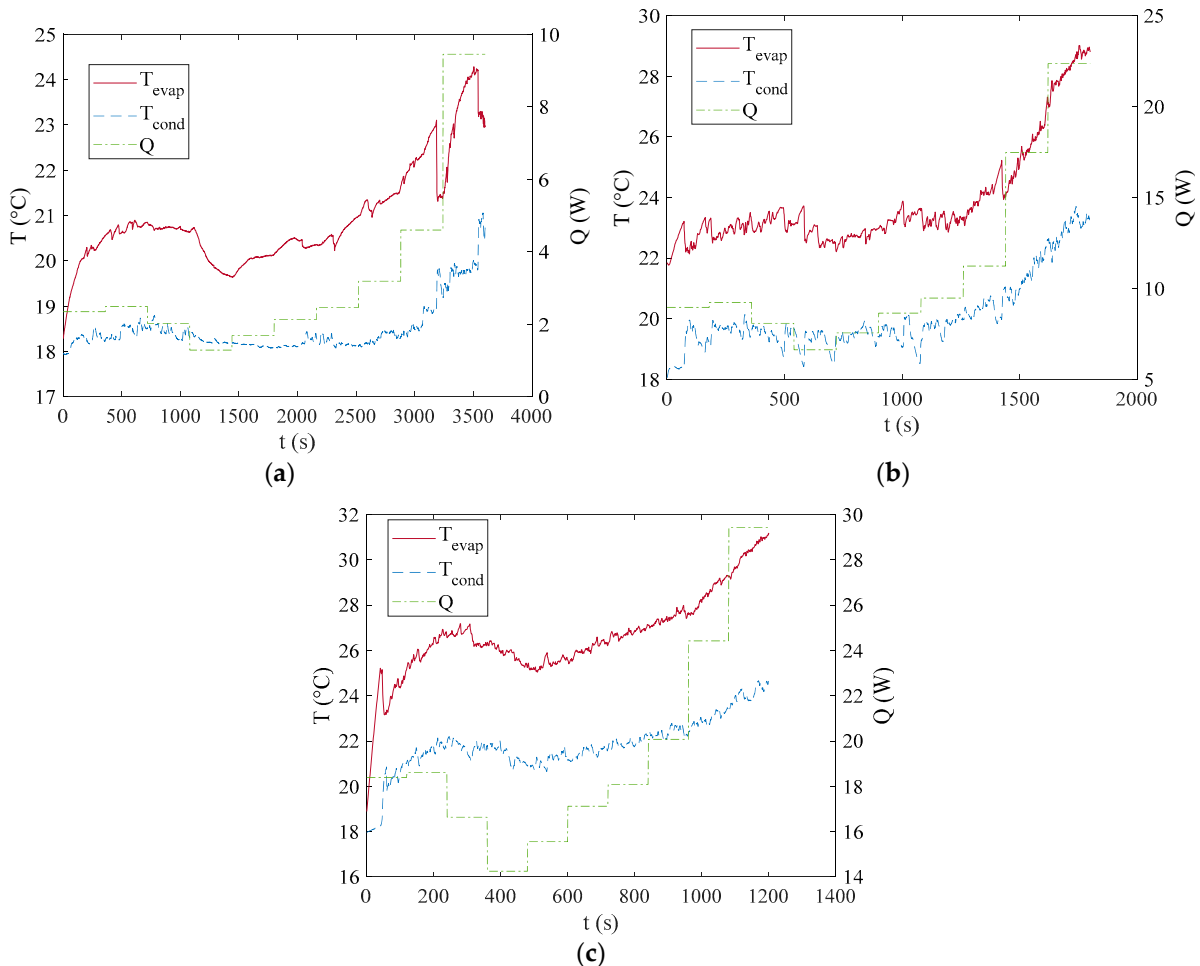


Figure 13. Average temperature at the evaporator and at the condenser for C1 (a), C2 (b) and C3 (c) discharging curves for the case of forced convection ($v = 2.5$ m/s).

For both the air velocity values the goal of keeping the temperature lower than the upper limit is achieved for all the C-rates, demonstrating the ability of the proposed device as an efficient passive battery thermal management system. As already said, all these tests were performed at ambient temperature of $18\text{ }^{\circ}\text{C}$, so further investigation varying the environmental temperature must be performed.

Since the aim of the device presented here is to provide a robust, efficient and totally passive battery cooling system for all the working conditions it is necessary to solve the bottleneck represented by the low heat transfer coefficient at the condenser section in natural convection, by increasing the surface heat transfer area. Indeed, the device must be able to guarantee the optimal working temperature range of the battery when forced convection is not available, avoiding the use of external power. This is, for instance, the case of a charging process where the vehicle is not moving and air flow cannot be naturally conveyed to the battery without using a fan and so consuming energy.

The heat transfer area at the condenser could be easily increased by adding fins as is reported in Figure 14.



Figure 14. Sketch of the PHP configuration with fins.

As it is possible to see from Figure 15 the simple configuration of fins on the battery pack of Figure 14 allows the temperature of the evaporator to remain under the upper limit.

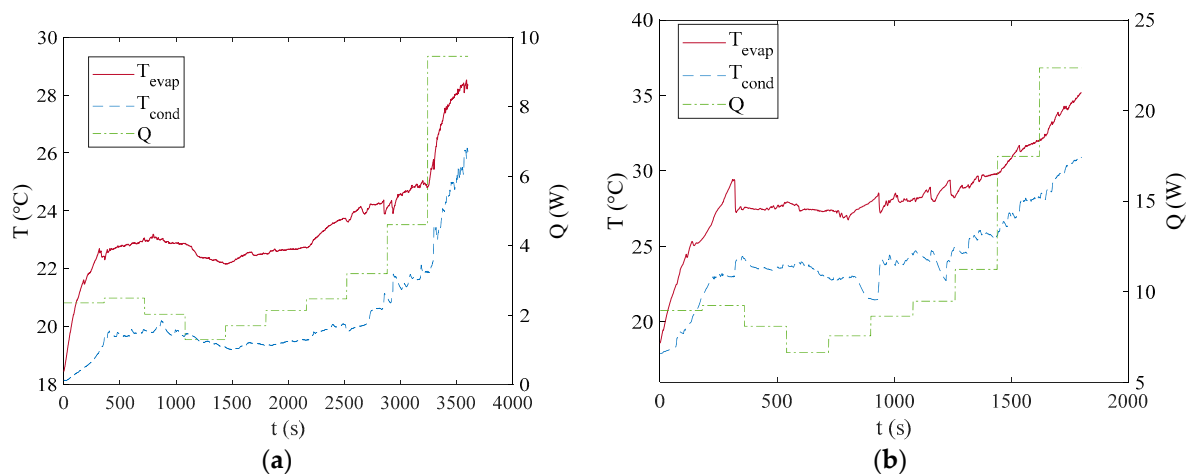


Figure 15. Cont.

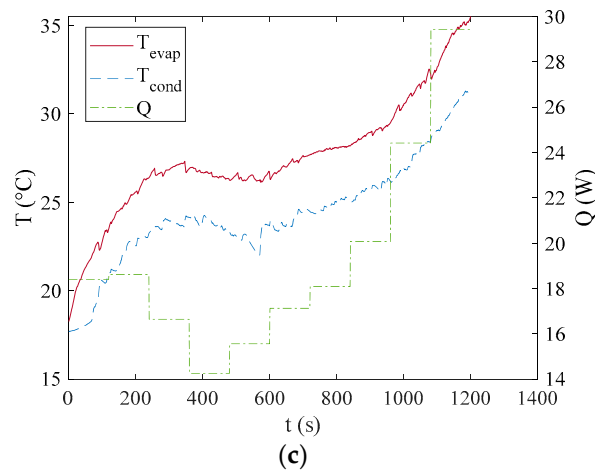


Figure 15. Average temperature at the evaporator and at the condenser for C1 (a), C2 (b) and C3 (c) discharging curves for the case of natural convection and PHP with fins.

3.3. Discharging Process at Extreme Environmental Temperature

After verifying the effective high potentiality of the proposed device it is necessary to explore the working limits of its application. On one side, low environmental temperature could be problematic for the activation of the oscillating mode of the PHP due to the higher viscosity of the fluid inside the device. On the opposite side, high environmental temperature of course represents a critical issue since the device is cooled by ambient air. To investigate these two conditions a thermal chamber (MPM Instruments—M400-TB) was adopted to simulate the environmental conditions of $T_{env} = 5\text{ }^{\circ}\text{C}$ and $T_{env} = 30\text{ }^{\circ}\text{C}$. The most critical configuration among the three studied, i.e., natural convection, was tested as the cooling mode at the condenser. The setup with fins was kept.

From Figure 16, where the average temperatures at the evaporator and at the condenser for the different C-rates for the case of $T_{env} = 5\text{ }^{\circ}\text{C}$ are reported, it is possible to notice that the device effectively counters problems of activation that seems to occur with some delay with respect to previous cases, i.e., at $t = 3200\text{ s}$ for C1, at $t = 1200\text{ s}$ for C2 and at $t = 500\text{ s}$ for C3. In any case, with this boundary condition no problem of overheating is faced, in fact, there could be the issue of not reaching the lower limit of the optimal working range. In this case an additional control system, such as a simple thermal resistance activated by the battery only when the temperature is lower than the lower limit, could be arranged.

The opposite problem is encountered for $T_{env} = 30\text{ }^{\circ}\text{C}$ where the upper temperature limit is approached both for the C2 case and C3 case (Figure 17). The positive aspect is that the limit is overcome only in the C3 case and the excess is limited to less than $3\text{ }^{\circ}\text{C}$. Of course, with an increase in the environmental temperature this problem will become greater, for instance, for $T_{env} = 35\text{ }^{\circ}\text{C}$ where the excess has been measured to be about $5\text{ }^{\circ}\text{C}$ for the C2 case and $8\text{ }^{\circ}\text{C}$ for the C3 case. Nevertheless, it must be considered that the natural convection represents the worst-case scenario for a battery of an electric vehicle as seen from Figures 11–13 and, moreover, until the environmental temperature remains below the upper limit it can be managed by increasing the heat transfer surface area with an improved battery pack with fins.

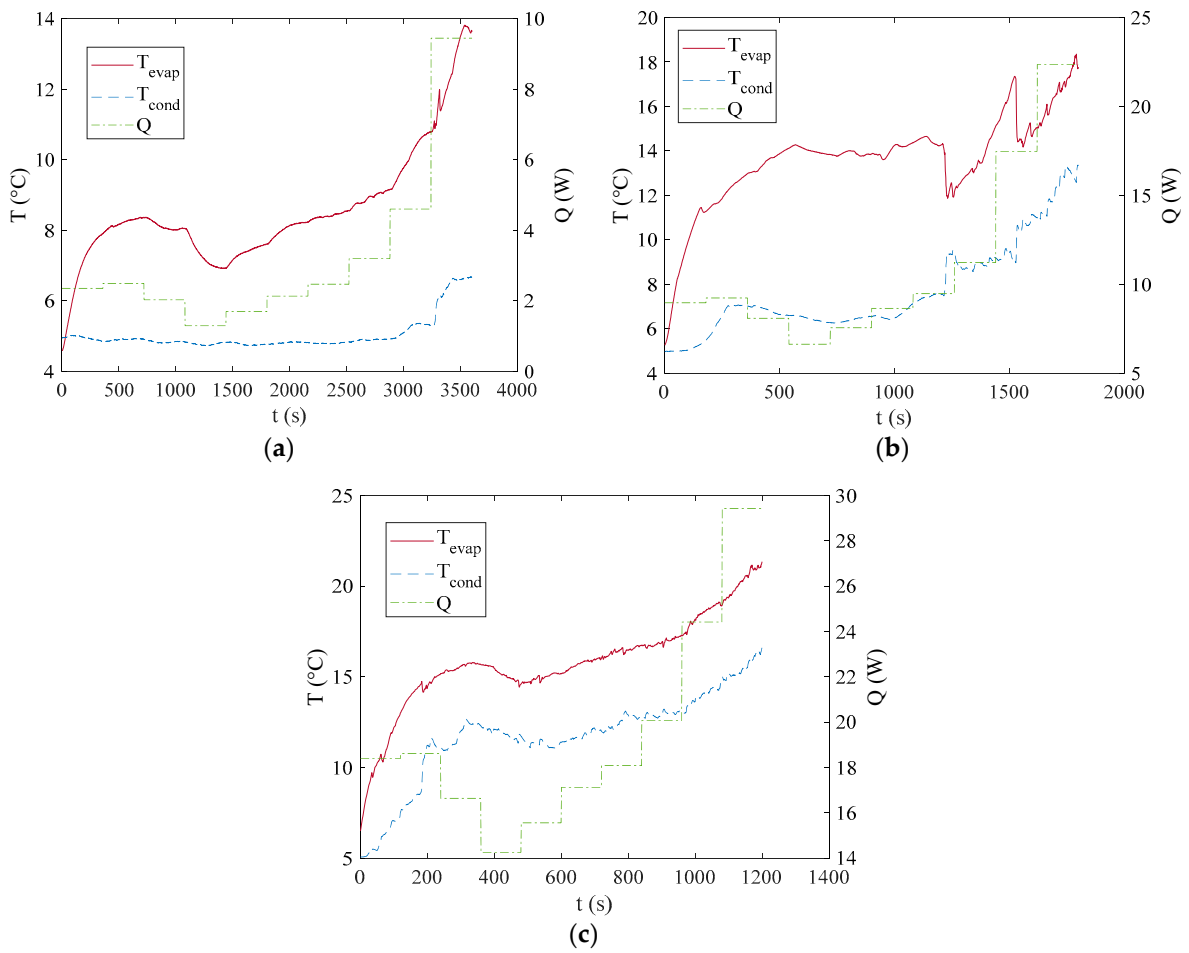


Figure 16. Average temperature at the evaporator and at the condenser for C1 (a), C2 (b) and C3 (c) discharging curves for the case of natural convection and PHP with fins at $T_{env} = 5^{\circ}C$.

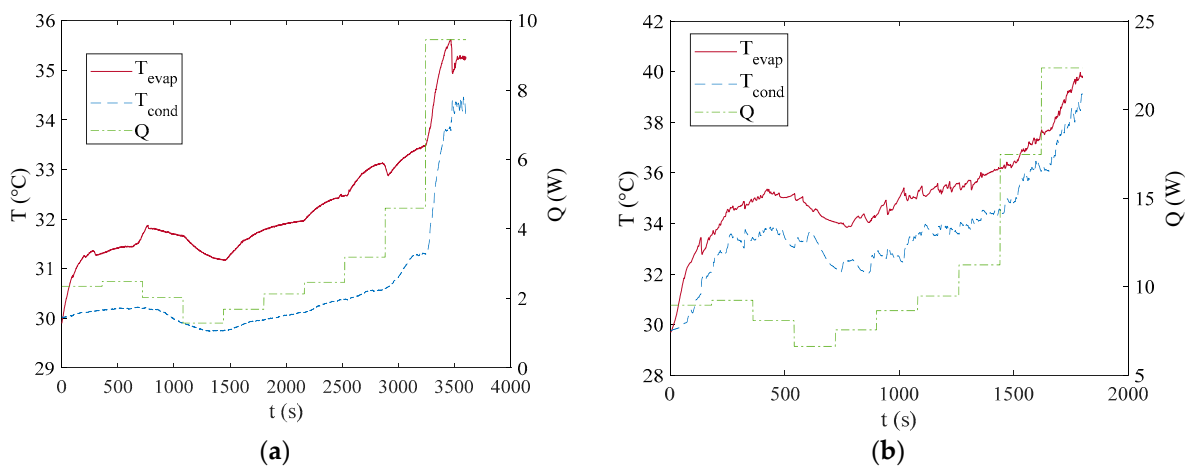


Figure 17. Cont.

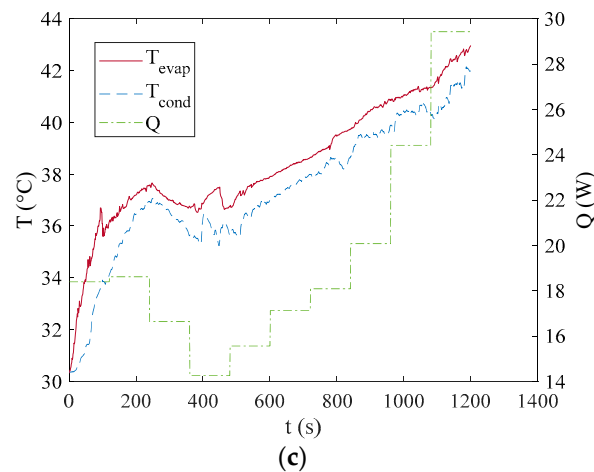


Figure 17. Average temperature at the evaporator and at the condenser for C1 (a), C2 (b) and C3 (c) discharging curves for the case of natural convection and PHP with fins at $T_{env} = 30\text{ }^{\circ}\text{C}$.

In conclusion, the presented device for the thermal management of batteries for electric vehicles was demonstrated to be effectively applicable to real working conditions, showing promising cooling performance.

4. Conclusions

In the present work an innovative cooling system for the thermal management of batteries for electric vehicles is presented and tested. At first the performance of the proposed PHP was evaluated in terms of average thermal resistance of the device under different boundary conditions and a wide spectrum of power input values. Then the PHP was tested by applying, as load at the evaporator section, the power distribution corresponding to three different discharging processes of a battery already tested in [23]. From the tests directly referring to an applicative case the proposed 3D PHP was shown to be able to keep the battery in the optimal working temperature range ($20\text{--}40\text{ }^{\circ}\text{C}$) for all the tested C-rates in the case of forced convection in a condition that simulates the case of a moving vehicle. The issue becomes more critical for the case of natural convection at the condenser section, a condition that can occur, for instance, during the charging phase. It requires the reducing of the thermal resistance at the condenser that can be successfully obtained by a fin pack. Then critical thermal conditions were analyzed, showing for all the studied cases optimal cooling ability and the possibility to offer a powerful solution for electrical battery thermal management. Finally, it is important to highlight that the fitting of the proposed thermal management system inside a vehicle is one of the issues that will be studied in future research activities, from a perspective of product engineering, considering that it would probably not have much bigger dimensions than an actual thermal management system based on liquid cooling, composed of the battery case, fluid circuit and radiator, or one based on air cooling that comprises a finned pack.

Author Contributions: Conceptualization, L.C., F.B., V.D. and L.G.; Methodology, L.C. and F.B.; Software, L.C. and M.M.; Validation, M.M.; Investigation, L.C., M.M., V.D. and L.G.; Resources, F.B.; Data curation, M.M.; Writing—original draft, L.C.; Writing—review & editing, M.M., F.B., V.D. and L.G.; Supervision, L.C.; Funding acquisition, L.C. All authors have read and agreed to the published version of the manuscript.

Funding: This research was granted by University of Parma through the action Bando di Ateneo 2021 per la ricerca co-funded by the MUR-Italian Ministry of Universities and Research (MUR)—D.M. 737/2021-PNR-PNRR-NextGenerationEU.

Data Availability Statement: The data presented in this study are available on request from the corresponding author.

Acknowledgments: The Authors would like to thank Alessandro Benelli for his support in the experimental tests.

Conflicts of Interest: The authors declare no conflict of interest.

Nomenclature

D	[m]	Diameter
h	[W/m ² °C]	Heat transfer coefficient
I	[A]	Discharge current
Q	[W]	Heat load
q	[W/m ²]	Heat flux
R	[°C/W]	Thermal resistance
T	[°C]	Temperature
t	[s]	Time
U_{OC}	[V]	Open circuit potential
V	[V]	Battery cell potential
v	[m/s]	Velocity
Subscripts		
$cond$		Condenser
env		Environment
eva		Evaporator

References

- Wada, M. Research and development of electric vehicles for clean transportation. *J. Environ. Sci.* **2009**, *21*, 745–749. [[CrossRef](#)] [[PubMed](#)]
- Albatayneh, A.; Juaidi, A.; Jaradat, M.; Manzano-Agugliaro, F. Future of Electric and Hydrogen Cars and Trucks: An Overview. *Energies* **2023**, *16*, 3230. [[CrossRef](#)]
- Speirs, J.; Contestabile, M.; Houari, Y.; Gross, R. The future of lithium availability for electric vehicle batteries. *Renew. Sust. Energ. Rev.* **2014**, *35*, 183–193. [[CrossRef](#)]
- Pesaran, A.A.; Santhanagopalan, S.; Kim, G.H. Addressing the impact of temperature extremes on large format Li-ion batteries for vehicle applications. In Proceedings of the 30th International Battery Seminar 2013, Fort Lauderdale, FL, USA, 11–14 March 2013.
- Ganesh, S.V.; D’Arpino, M. Critical Comparison of Li-Ion Aging Models for Second Life Battery Applications. *Energies* **2023**, *16*, 3023. [[CrossRef](#)]
- Park, H. A design of air flow configuration for cooling lithium-ion battery in hybrid electric vehicles. *J. Power Sources* **2013**, *239*, 30–36. [[CrossRef](#)]
- Wang, X.; Liu, S.; Zhang, Y.; Lv, S.; Ni, H.; Deng, Y.; Yuan, Y. A review of the power battery thermal management system with different cooling, heating and coupling system. *Energies* **2022**, *15*, 1963. [[CrossRef](#)]
- Nelson, P.; Dees, D.; Amine, K.; Henriksen, G. Modeling thermal management of lithium-ion PNGV batteries. *J. Power Sources* **2002**, *110*, 349–356. [[CrossRef](#)]
- Hajjalibabaei, M.; Saghier, M.Z.; Bicer, Y. Comparing the Performance of a Straight-Channel Heat Sink with Different Channel Heights: An Experimental and Numerical Study. *Energies* **2023**, *16*, 3825. [[CrossRef](#)]
- Huo, Y.; Rao, Z.; Liu, X.; Zhao, J. Investigation of power battery thermal management by using mini-channel cold plate. *Energy Convers. Manag.* **2015**, *89*, 387–395. [[CrossRef](#)]
- An, Z.; Jia, L.; Li, X.; Ding, Y. Experimental investigation on lithium-ion battery thermal management based on flow boiling in minichannel. *Appl. Therm. Eng.* **2017**, *117*, 534–543. [[CrossRef](#)]
- Mayer, B.; Schier, M.; Friedrich, H.E. Stand-Alone Battery Thermal Management for Fast Charging of Electric Two Wheelers Integrated Busbar Cooling. *World Electr. Veh. J.* **2019**, *10*, 37. [[CrossRef](#)]
- Hirano, H.; Tajima, T.; Hasegawa, T.; Sekiguchi, T.; Uchino, M. Boiling Liquid Battery Cooling for Electric Vehicle, In Proceedings of the 14th ITEC Asia-Pacific, Beijing China, 31 August–3 September 2014.
- Zhu, L.; Boehm, R.F.; Wang, Y.; Halford, C.; Sun, Y. Water immersion cooling of PV cells in a high concentration system. *Sol. Energy Mater. Sol. Cells* **2011**, *95*, 538–545. [[CrossRef](#)]
- Duan, X.; Naterer, G. Heat transfer in phase change materials for thermal management of electric vehicle battery modules. *Int. J. Heat. Mass. Transf.* **2010**, *53*, 5176–5182. [[CrossRef](#)]
- Budiman, A.C.; Azzopardi, B.; Perdana, M.A.; Kaleg, S.; Hadiastuti, F.S.; Hasyim, B.A.; Hapid, A. Phase Change Material Composite Battery Module for Thermal Protection of Electric Vehicles: An Experimental Observation. *Energies* **2023**, *16*, 3896. [[CrossRef](#)]
- Wang, J.; Gan, Y.; Liang, J.; Tan, M.; Li, Y. Sensitivity analysis of factors influencing a heat pipe-based thermal management system for a battery module with cylindrical cells. *Appl. Therm. Eng.* **2019**, *151*, 475–485. [[CrossRef](#)]

18. Gan, Y.; He, L.; Liang, J.; Tan, M.; Xiong, T.; Li, Y. A numerical study on the performance of a thermal management system for a battery pack with cylindrical cells based on heat pipes. *Appl. Therm. Eng.* **2020**, *179*, 115740. [[CrossRef](#)]
19. Lisbona, D.; Snee, T. A review of hazards associated with primary lithium and lithium-ion batteries. *Process Saf. Environ. Prot.* **2011**, *89*, 434–442. [[CrossRef](#)]
20. Khandekar, S.; Groll, M. On the definition of pulsating heat pipes: An overview. In Proceedings of the 5th Minsk International Conference, Minsk, Belarus, 8–11 September 2003.
21. Pagliarini, L.; Cattani, L.; Slobodeniuk, M.; Ayel, V.; Romestant, C.; Bozzoli, F.; Rainieri, S. Novel Infrared Approach for the Evaluation of Thermofluidic Interactions in a Metallic Flat-Plate Pulsating Heat Pipe. *Appl. Sci.* **2022**, *12*, 11682. [[CrossRef](#)]
22. Iwata, N.; Bozzoli, F.; Pagliarini, L.; Cattani, L.; Vocale, P.; Malavasi, M.; Rainieri, S. Characterization of thermal behavior of a micro pulsating heat pipe by local heat transfer investigation. *Int. J. Heat. Mass Transf.* **2022**, *196*, 123203. [[CrossRef](#)]
23. Yu, X.; Chen, R.; Gan, L.; Li, H.; Chen, L. Battery safety: From lithium-ion to solid-state batteries. *Engineering* **2023**, *21*, 9–14. [[CrossRef](#)]
24. Tufail, M.K.; Zhai, P.; Jia, M.; Zhao, N.; Guo, X. Design of Solid Electrolytes with Fast Ion Transport: Computation-Driven and Practical Approaches. *Energy Mater. Adv.* **2023**, *4*, 0015. [[CrossRef](#)]
25. Alaoui, C. Modular energy efficient and solid-state Battery Thermal Management System. In Proceedings of the 2017 International Conference on Wireless Technologies, Embedded and Intelligent Systems (WITS), Fez, Morocco, 19–20 April 2017; pp. 1–6.
26. Giammichele, L.; D'alessandro, V.; Falone, M.; Ricci, R. Preliminary analysis of a novel battery thermal management system based on a low boiling dielectric fluid. In *IOP Conference Series*; IOP Publishing: Bristol, UK, 2022.
27. Zhang, Y.; Faghri, A. Advances and unsolved issues in pulsating heat pipes. *Heat Transf. Eng.* **2008**, *29*, 20–44. [[CrossRef](#)]
28. Winkler, M.; Rapp, D.; Mahlke, A.; Zunftmeister, F.; Vergez, M.; Wischerhoff, E.; Schäfer-Welsen, O. Small-sized pulsating heat pipes/oscillating heat pipes with low thermal resistance and high heat transport capability. *Energies* **2020**, *13*, 1736. [[CrossRef](#)]
29. Yang, K.S.; Jiang, M.Y.; Tseng, C.Y.; Wu, S.K.; Shyu, J.C. Experimental investigation on the thermal performance of pulsating heat pipe heat exchangers. *Energies* **2020**, *13*, 269. [[CrossRef](#)]
30. Tseng, C.Y.; Wu, H.M.; Wong, S.C.; Yang, K.S.; Wang, C.C. A novel thermal module with 3-D configuration pulsating heat pipe for high-flux applications. *Energies* **2018**, *11*, 3425. [[CrossRef](#)]
31. Bevington, P.R. *Data Reduction and Error Analysis for the Physical Sciences*; McGraw-Hill: New York, NY, USA, 1969.
32. Błasiak, P.; Opalski, M.; Parmar, P.; Czajkowski, C.; Pietrowicz, S. The thermal—Flow processes and flow pattern in a pulsating heat pipe—Numerical modelling and experimental validation. *Energies* **2021**, *14*, 5952. [[CrossRef](#)]
33. Giammichele, L.; D'Alessandro, V.; Falone, M.; Ricci, R. Experimental study of a direct immersion liquid cooling of a Li-ion battery for electric vehicles applications. *Int. J. Heat Technol.* **2022**, *40*, 5952. [[CrossRef](#)]
34. Bernardi, D.; Pawlikowski, E.; Newman, J. A General Energy Balance for Battery Systems. *Electrochem. Soc.* **1985**, *132*, 5–12. [[CrossRef](#)]
35. Andrzejczyk, R. Experimental investigation of the thermal performance of a wickless heat pipe operating with different fluids: Water, ethanol, and ses36. analysis of influences of instability processes at working operation parameters. *Energies* **2018**, *12*, 80. [[CrossRef](#)]

Disclaimer/Publisher's Note: The statements, opinions and data contained in all publications are solely those of the individual author(s) and contributor(s) and not of MDPI and/or the editor(s). MDPI and/or the editor(s) disclaim responsibility for any injury to people or property resulting from any ideas, methods, instructions or products referred to in the content.